

1 Porosity preservation due to grain coating illite/smectite: evidence from Buchan
2 Formation (Upper Devonian) of the Ardmore Field, UK North Sea

3

4 Longxun Tang^{1*}, Jon Gluyas¹, Stuart Jones¹

5 1. Department of Earth Sciences, Durham University, South Road, Durham, DH1 3LE,
6 United Kingdom

7 *Corresponding author Email: longxun.tang@outlook.com

8

9

10 **Abstract:** The Buchan Formation sandstone reservoirs from the Ardmore Field in the UK
11 North Sea are fluvial-aeolian deposits and provide examples of porosity preservation in
12 deeply-buried reservoirs (2.7 – 3.2 km) caused by grain-coating illite/smectite (I/S). Here,
13 high reservoir quality commonly correlates with the occurrence of grain-coating I/S and
14 consequent inhibition of quartz cementation in the aeolian dune and interdune sandstones.
15 Porosity is lower in fluvial sandstones lacking grain coating I/S but with intense quartz
16 overgrowths. We propose that the presence of I/S reflects concentration of the smectitic-rich
17 clay bearing water which would have been the deposits of the interdune and/or distal sector
18 of fluvial distributary system, and were introduced into aeolian deposits by mechanical
19 infiltration. Petrographic relationships indicate that these coatings grew mainly before the
20 mechanical compaction as the clays occur at grain contacts. The use of empirical model
21 suggested that about 6 – 7% porosity have been preserved. The burial-thermal history of the
22 Ardmore area contributed to the high quality reservoir because throughout much of the time
23 since deposition, the Devonian sandstones have been little buried. Only from the Palaeogene
24 the reservoir temperatures exceeded about 70°C and rapidly buried to today’s maximum
25 depth, which have minimized the negative effect generally ascribed to smectitic clays on
26 reservoir quality. The circumstances of porosity preservation shown in this study may be
27 unusual, but nonetheless have profound consequences for exploration. It is possible to
28 identify new Buchan Formation prospects in areas hitherto dismissed because they were
29 generally assumed to be poor reservoir.

30 **Key words:** Grain coating illite/smectite, Upper Devonian, Clay infiltration, Porosity
31 preservation, UK North Sea

1. Introduction

32 Quartz cement is one of the dominant porosity reducing agents in many reservoir
33 sandstones, but other factors such as grain size, sorting, clay content, mechanical compaction,
34 pore fluid pressure, early cementation and authigenic clay minerals also play a critical role
35 (Worden and Morad, 2000). Different types of grain coatings have been identified to inhibit
36 or reduce quartz cementation. The basic mechanism of inhibiting quartz overgrowth is that
37 the grain coatings covered the nucleation site on the host grains and the authigenic quartz
38 could not nucleate on or through the coatings (Pittman, 1972). The most effective grain
39 coating mineral is said to be micro-quartz (Aase et al., 1996) and for the grain coating clays,
40 authigenic chlorite is commonly reported as a preserver (e.g. Pittman and Lumsden, 1968;
41 Ehrenberg, 1993; Berger et al., 2009; Stricker and Jones, 2016). Illite is less frequently
42 reported as grain coatings that preserve porosity (Storvoll et al., 2002) but frequently cited as
43 the cause of permeability destruction (Robinson et al., 1993). Smectitic clay is commonly
44 regarded as having negative effects on reservoir quality due to its water-sensitive swelling
45 property (Gray and Rex, 1965), and it commonly transforms to fibrous/hairy illite in a
46 potassium-rich pore fluids. Precipitation of illite usually causes significant permeability
47 reduction (Almon and Davies, 1981; Le Gallo et al., 1998; Wilson et al., 2014).

48 The oil reservoirs in the Ardmore Field, UK Block 30/24, UK North Sea, are hosted in
49 Permian Zechstein carbonates, Permian Rotliegend sandstones and Upper Devonian Buchan
50 Formation sandstones (Gluyas et al., 2005). The two Permian units have been studied in a
51 number of publications (e.g. Nagtegal, 1979; Glennie and Provan, 1990; Purvis, 1992;
52 Howell and Mountney, 1997; Leveille et al., 1997; Sweet, 1999); however, the deeper and
53 older Buchan Formation sandstones (2.7 – 3.2 km TVDSS) are poorly understood but have
54 also been proven to be an important hydrocarbon reservoir in the North Sea (e.g. Edwards,
55 1991; Knight et al., 1993; Gambaro and Currie, 2003; Gluyas et al., 2005).

56 In this study, we discovered that the aeolian-associated sandstones with grain coating
57 illite/smectite (I/S) usually have anomalously high porosity and permeability, while quartz
58 overgrowth is almost absent in this sandstone type. Conversely, the fluvial facies without
59 thick and continuous I/S coatings are usually cemented by extensive quartz overgrowth, and
60 commonly show poor, or at best, moderate reservoir quality. Therefore, this study focused on
61 the following points and questions: 1) why is the grain coating I/S only presented in aeolian
62 sandstones and how did it form? and 2) is it possible to quantitatively evaluate the porosity
63 preserving effect of I/S grain coatings? The positive effect of grain coating I/S can be
64 expected to occur only under particular circumstances, but in such cases it can have profound
65 consequences for exploration. This study has broad implications for future exploration,
66 appraisal and production of Devonian reservoirs within this area.

67 **2. Geological Setting**

68 **2.1 Tectonic Setting**

69 The Ardmore Field is located on the Argyll Ridge, a large SW-NE trending Palaeozoic age
70 tilted fault block on the south-western flank of the Central Graben in Block 30/24, UK North
71 Sea, about 350 km south-east from Aberdeen. The field is located in a horst feature with the
72 crest in the north and fault closure to the north-east. It measures 2.5 km wide and 6 km long
73 (Fig. 1a). A combination of dip and faulting defines the limits of the field on the north-west
74 and south-east flanks, while dip closure defines the southern limits of the field. The major
75 fault trends are in two main directions, WNW–ESE cut by NE-SW faults (Fig. 1b). The top
76 seal is provided by Triassic shale in the far west, Jurassic shale in the mid-part of the field
77 and impermeable Chalk at the north-eastern crest (Gluyas et al., 2005). The trap relies heavily
78 on the major NE-SW trending graben edge faults to the northeast and southwest of the field
79 while dip closure occurs to the northwest and west.

80 2.2 Stratigraphy

81 The Devonian sequence in the Ardmore Field comprises a succession of the Middle
82 Devonian Kyle limestone and Upper Devonian Buchan Formation. The succession dips to the
83 south-west, and is separated from the Permian by a palaeo-topographic unconformity, in
84 which successively younger stratigraphic units in the Devonian sub crop towards the south-
85 west. Although the pre-Permian surface has topography it also dips to the SW, this has the
86 effect of making the oldest part of the Buchan Formation subcrop the unconformity in the NE
87 of the field and thus the youngest Devonian in the SW slightly deeper (Fig. 1b).

88 The Upper Devonian Buchan Formation comprises a thick, generally upward-coarsening
89 succession of shales of mixed shallow marine and sabkha environment at the base, passing
90 upwards into mainly fluvial and aeolian sandy sediments (Fig. 2). The whole Buchan
91 succession lacks clear seismic stratigraphic markers, a combination of log and core data has
92 been used to divide the stratigraphic units for the Upper Devonian group: B01 is the oldest
93 unit overlying the Middle Devonian Limestone, and B11 is the youngest unit (Gluyas et al.,
94 2005). In the absence of bio-stratigraphic data, sedimentary structures and lithofacies
95 associations have been applied to help correlation (Gluyas et al., 2005). The total thickness of
96 the Buchan Formation is not documented due to the combination of erosion below the
97 Devonian-Permian unconformity, lateral thickness variation and incomplete well penetrations.
98 The estimated thickness is about 250 – 800 m according to the seismic profile (Fig. 1c).

99 Units B01, B02, B03, B05 and B06 are equivocal about their origin due to the insufficient
100 core coverage. The core description revealed the presence of two main sedimentary facies
101 within the Buchan formation (Robson, 1991; Gluyas et al., 2005). Braided fluvial facies is the
102 volumetrically major type (approx. 70%) and consists of multiple fining-upward sequences
103 (not shown in the Fig. 2), each sequence is commonly composed of: 1) sand-supported

104 conglomerates at the cycle base with thickness around 0.5 – 1 m, the quartz and muddy clast
105 pebbles (1 – 3 cm in diameter) are sub-angular to sub-rounded and show roughly imbricated
106 alignment, which indicates the thin basal lag deposit within a channel (CHC); 2) fine to
107 medium-grained, moderately sorted sandstones with trough cross bedding, planar cross
108 bedding and horizontal laminations are the dominant type within the fining-upward cycle,
109 representing various channel bar deposits (CHB) such as residual dunes, linguoid and
110 transverse bars, and planar bed flows; and 3) laminated fine-grained sediments with soft
111 sediment deformation usually form the top of the sequence, which indicate the decrease of
112 flow velocity such as sand flat (SF) or channel abandonment (CHA) and usually occur at the
113 top of the cycle with 0.5 m and up to 3 m thick.

114 The aeolian facies is the volumetrically minor type (approx. 30%) and composed of well
115 sorted, medium-grained, pin-stripe laminated sandstones and fine-grained, discontinuous
116 wavy laminated sandstones, which represents an interbedded dune (AD) and interdune (ID)
117 deposits. Overall, the known units comprise a vertically fluvial (B04, approx. 100 m)-aeolian
118 (B07 and B08, approx. 50 m)-fluvial (B09, B10 and B11, approx. 240 m) variation, which
119 generally represents a progradation-retreat-progradation cycle of the alluvial fan-based
120 braided system with aeolian deposits occurring mainly between two main progradation
121 periods.

122 **2.3 Previous study on Ardmore Field**

123 The field is charged by Upper Jurassic Kimmeridge Clay in the northeast of Ardmore, which
124 indicates these three reservoirs are in hydraulic connection (Gluyas et al., 2005). The Buchan
125 Formation is composed chiefly of a sand-dominated unit deposited in a braided fluvial and
126 aeolian environment during a hot and semi-arid to arid period (Gluyas et al., 2005; Kearsey et
127 al., 2015). Gluyas et al. (2005) reported the conventional core analysis data for Buchan

128 Formation sandstones, porosity ranges between 1% and 28% while permeability varies
129 between <1 mD and >5000 mD. The main influences on reservoir quality reduction were
130 mechanical compaction, extensive quartz overgrowth and dolomite cementation (Bifani and
131 Smith, 1985).

132 **3. Dataset And Methodology**

133 A total of 190 samples were taken from BGS and EnQuest core stores. Cores from five
134 wells (30/24-05, 30/24-20z, 30/24-28, 30/24-31, 30/24-34) in the Buchan Formation ranging
135 from 2650 m to 3150 m (TVDSS) were logged. The porosity and permeability data were
136 provided by EnQuest internal reports. Porosity was determined via direct measurement of
137 grain volume and bulk volume by helium expansion in a Boyle's Law porosimeter; the
138 permeability data was determined by use of a nitrogen permeameter at a confining pressure of
139 400 psig and are Klinkenberg-corrected.

140 Thin-section petrography was used to determine the rock mineralogy, diagenetic features,
141 pore types and clay distribution in the pore spaces. One hundred and one thin sections (14
142 from well 30/24-05, 16 from well 30/24-20z, 38 from well 30/24-28, 16 from well 30/24-31
143 and 17 from well 30/24-34) were used for petrographic analysis and point counting. The
144 samples were impregnated with blue-dyed resin in order to identify porosity.

145 At least 300 points were counted in each thin section to identify detrital and authigenic
146 phases, including the clay aggregates which are larger than 0.05 mm in size (pore space is
147 excluded). This number of point counts per thin section has a standard deviation of 5.5% or
148 less (at the 95% confidence level) for any measured volumetric percentage of mineral or
149 porosity components (Stanton and Wilson, 1994). The point count results, petrographic
150 information, and laboratory measured porosity/permeability are presented in Supplementary
151 table 1.

152 Microstructural observation was obtained in both secondary and backscattered electron
153 imaging, with a Hitachi SU70 scanning electron microscope (SEM). Typical voltage for thin
154 sections was obtained at 15 Kev, 0.73 nA together with an analytical working distance of 15
155 mm. The electron microscope is equipped with an Oxford Instrument Aztec microanalysis
156 system and Silicon drift (SDD) EDX detector X-max 50. Thin sections were carbon coated at
157 30 nm (Cressington Scientific 108 evaporating system A) in order to obtain large area “Phase
158 Maps” which were achieved using Phase ID within Aztec 3.3 software. Rock chip samples
159 from both fluvial and aeolian sandstones were Au/Pd coated at 35 nm (Cressington Scientific
160 108 Auto sputter coater) for optimum imaging resolution at 5 to 8 Kev.

161 To identify and quantify the clay mineralogy, six samples were chosen for XRD analysis
162 (4 from grain coated aeolian sandstone samples, 2 from fluvial sandstone samples with quartz
163 and dolomite cements and without grain coatings). The bulk rock was disaggregated by
164 gentle crushing and suspend in distilled water. After allowing the coarse grains to settle for 3
165 hours, the clay in suspension was decanted in the centrifuge for 4.8 minutes at 1000 rpm, and
166 this process is performed 3 times. Clay with less than 2 microns was tested after being air
167 dried, solvation with glycerol and heating at 500°C for 2 hours.

168 **4. Results**

169 **4.1 General Petrographic Descriptions**

170 **4.1.1 Detrital mineralogy**

171 The studied Buchan Formation sandstones are litharenite to sub-litharenite and minor
172 quartz-arenite based on Folk (1957), with an overall average composition of $Q_{78.3}F_{2.9}R_{18.8}$.
173 The average composition for fluvial sandstones is $Q_{76.1}F_{3.3}R_{20.7}$ (Fig. 3a); aeolian sandstones
174 have an average composition of $Q_{82.1}F_{2.4}R_{15.6}$ (Fig. 3b). Texturally, the fluvial sandstones are

175 relatively immature and fine to medium grained, sorting ranges from poor to moderate and
176 roundness of grains varies from sub-angular to sub-rounded. Grains are tightly compacted
177 showing long and curved grain contacts. Conversely, the fine to medium grained aeolian
178 sandstones are more mature, sorting ranges from moderate to good and roundness of grains
179 varies from sub-rounded to rounded, and the grain contacts are commonly point to long.

180 In all samples, quartz is the dominant grain type (25 – 92.5%). Most quartz grains are
181 monocrystalline (Fig. 4a), some of them showing little to moderate undulose extinction (Fig.
182 4b). Polycrystalline quartz is a minor constituent and only found in fine pebble grains (Fig.
183 4c). Feldspar is commonly present in trace amount and up to 7%, the main type is microcline
184 with polysynthetic twinning (Fig. 4d). The feldspars occur as both fresh (Fig. 4d) and
185 kaolinitized grains (Fig. 4e). Most mica grains are muscovite presenting in all the samples
186 and comprising up to 13%. Micas show variable amounts of distortion (Fig. 4b). Rock
187 fragments (Fig. 4f) are mainly micaceous and illitic mud clasts, fine-grained metamorphic
188 and volcanic fragments are present in trace quantities. The abundance of rock fragments is
189 highly variable (1 – 69%) and related to different sub-facies: CHB have lower average rock
190 fragments (11%) among all fluvial sub-facies (15% in CHC, 16% in SF and 27% in CHA). In
191 the aeolian facies, aeolian dune sandstones have a lower average rock fragments (13%) than
192 the interdune deposits (16%).

193 In both fluvial and aeolian sandstones, pore space mainly consists of primary intergranular
194 pores, secondary inter- and intragranular pores and intra-crystalline micro pores. The
195 polygonal intergranular pores are the main type (more than 90% among all pore space) and
196 range in sizes from 5 – 200 μm . The secondary pores (less than 10% among all pore space)
197 are mainly contributed from framework-grain dissolution (e.g. dissolution of detrital
198 feldspars), and dissolution of dolomite cement can be found in trace amounts. The intra-

199 crystalline micro pores (negligible among all pore space) mainly consist of micro pores in
200 clay minerals (e.g. kaolinite, illite, smectite) and range in size from 0.1 – 5 µm.

201 **4.1.2 Authigenic mineralogy**

202 Authigenic minerals in the studied sandstones are mainly dolomite, quartz overgrowth,
203 kaolinite, illite and I/S. The kaolinite, illite and quartz overgrowth are usually associated with
204 fluvial sandstones, while I/S are only found in aeolian sandstones.

205 Dolomite is the prevalent cement in the Buchan Formation sandstones ranging from 0 – 36%
206 with an average value of 5.7%, and are commonly iron-stained. It is usually presented as thin
207 bands of disseminated red-brown stained nodules in hand specimen with a size of up to 2 mm
208 (Fig. 5a). Thin section observation reveals a rhombic shape with clear rims and cloudy centre
209 (Fig. 5b) and poikilotopic structure (Fig. 5c).

210 Quartz overgrowth is present primarily as syntaxial cement forming incomplete or
211 complete rims around quartz grains (Figs. 4a and 5d). Boundaries between detrital quartz
212 grains and overgrowth cements are visible due to the presence of inclusions along grain
213 boundaries. Quartz overgrowths are widely distributed in the fluvial sandstone samples (up to
214 6%, average 3%) and is almost absent in aeolian samples, except a few of them (5 out of 36)
215 have trace amount of quartz overgrowth up to 1% (Supplementary table 1). Kaolinite and
216 authigenic illite are the two main clay types in fluvial sandstones. Kaolinite ranges from 0%
217 and up to 15% with an average amount of 6%, mainly occurs as euhedral pseudo-hexagonal
218 plates and vermicular or booklet aggregates filling primary pores (Fig. 5e). In the aeolian
219 sandstones, kaolinite is in minor amount ranged from 0% to 6% (average 2%). Illite has a
220 range from 0% and up to 7% with an average amounts of 2% and occurs as fibrous or hairy
221 crystals mainly nucleated on kaolinite (Fig. 5f) and shows a pore-bridging habit (Fig. 5g).

222 Illite/smectite (I/S) has been identified by XRD (Table. 1) and EDX analysis (Fig. 5k). It
223 is the most important clay type in the studied aeolian sandstones although it is only present in
224 minor amounts (0.5 – 5%). The thin section and SEM observations illustrate that the I/S is
225 presenting in two forms: 1) grain coating I/S (Figs. 5h, 5i) commonly occurs as cornflake or
226 honeycomb morphology with filamentous terminations, and consists of a 1 – 5 μm thick rim
227 coating all the detrital grains in aeolian sandstones; it is absent in fluvial sandstones. It is also
228 observed that quartz overgrowth are absent in aeolian sandstones where uniform and robust
229 grain coating I/S has developed; and 2) pore-filling I/S (Fig. 5i, 5j), commonly presenting as
230 flocculent aggregates existing in the intergranular pore space of aeolian sandstones, and is
231 also absent in fluvial sandstones. To evaluate the development, coverage and continuity of
232 the grain coating I/S, the mineral phase map has been created for a typical aeolian dune
233 sample (Figs. 6a and 6b). Figure 6b clearly displayed that nearly all the grains are coated by
234 well-developed and continuous grain coating I/S, the visual grain coating coverage is nearly
235 100%.

236 In both sandstone types, chlorite is subordinate and present in trace amounts (0.1 - 0.5%)
237 which is confirmed by XRD analysis (Table 1).

238 **4.2 Porosity and Permeability**

239 The Buchan Formation sandstones have a wide range of porosity and permeability ($\phi = 1 -$
240 28% and $K = 0.1 - 5290$ mD). Porosity and permeability are well correlated in most of the
241 samples (in fluvial samples, $R^2 = 0.68$; in aeolian samples, $R^2 = 0.89$; in all samples, $R^2 = 0.74$)
242 inferred that the factors affecting porosity would also affect permeability (Fig. 7a).

243 For the fluvial units including B04, B09, B10 and B11 (Figs. 7b-7e), the porosity ranges
244 from 0.1% to 23.1% (arithmetic mean 12.7%), and the permeability ranges from 0.2 mD to
245 1240 mD (arithmetic mean 147.7 mD, geometric mean 5.41 mD). For the aeolian units B07

246 and B08 (Fig. 7f), the porosity ranges from 5.1% to 28% (arithmetic mean 20.2%), and the
247 permeability ranges from 0.2 mD to 5290 mD (arithmetic mean 740.6 mD, geometric mean
248 64.9 mD).

249 **4.3 Porosity loss evaluation**

250 Calculation on porosity loss from compaction (COPL) and cementation (CEPL) is a good
251 way to calculate the effect of compaction and cementation on reducing porosity. These two
252 parameters were firstly proposed by Lundergard (1992), and a useful parameter compaction
253 index (I_c), can be calculated using following equations:

$$\text{COPL} = P_i - \left(\frac{(100 - P_i) \times \text{IGV}}{100 - \text{IGV}} \right). \quad (1)$$

$$\text{CEPL} = (P_i - \text{COPL}) \times \left(\frac{C}{\text{IGV}} \right). \quad (2)$$

$$I_c = \frac{\text{COPL}}{\text{COPL} + \text{CEPL}}. \quad (3)$$

254 Where P_i is the assumed initial porosity, the intergranular volume (IGV) is calculated by
255 adding up the measured porosity and the total cement volume C . The calculation of COPL
256 and CEPL are only accurate when three conditions are met: 1) the assumed initial porosity P_i
257 is appropriate; 2) the amount of cement produced by local grain dissolution is negligible or
258 known; and 3) the amount of framework exported by dissolution is negligible or known
259 (Lundergard, 1992). The compaction index (I_c) equals 1.0 when all porosity loss is due to
260 mechanical compaction, and equals 0.0 when all porosity loss is due to cementation. In this
261 study, we employ the estimated P_i for loose sand according to Beard and Weyl (1973), the
262 assumed P_i for the fine-medium grained, moderately sorted fluvial sandstones is 34.8%, and
263 for the fine-medium grained, well sorted aeolian sandstones, P_i is 37.8%.

264 The results (Supplementary table 2) show that compaction has reduced more porosity in
265 aeolian sandstones than in fluvial sandstones: the COPL value is 14.82% (accounted for

266 39.21% on initial porosity, average $I_c = 0.73$) in aeolian sandstone samples. 10.06%
267 (accounted for 28.91% on initial porosity, average $I_c = 0.44$) in fluvial sandstone samples,
268 respectively. It is also worthy to note that the COPL of fluvial samples has a larger range (0 –
269 29%) than aeolian samples (3.5 – 22.8%).

270 The CEPL results suggest that fluvial sandstones suffered much more porosity loss from
271 cementation (average 12.71%, accounted for 36.52% on initial porosity) than aeolian
272 sandstones (average 5.63%, accounted for 14.89% on initial porosity).

273 **4.4 Burial-thermal history**

274 The 1D burial history was modelled using Schlumberger petroleum systems modelling
275 software PetroMod (V2014.1). Several heat flow histories of the Central Graben, to be more
276 specifically, UK Quadrant 30 in the UK North Sea have been employed for the modelling
277 (Swarbrick et al., 2000; Carr, 2003; Di Primio and Neumann, 2008). Figure 8 is a burial-
278 temperature history for the Buchan Formation in the Ardmore Field which is generally
279 similar to burial histories presented in other studies of Central Graben (Nguyen et al., 2013).
280 The Buchan Formation in the Ardmore Field was at consistently shallow burial depth and low
281 temperature (< 1.5 km and < 70°C) until Paleogene, and then rapidly buried into current
282 maximum depth (2.7 – 3.2 km) and temperature (approx. 115°C) within a short period (less
283 than 70 million years).

284 **5. Paragenesis**

285 The relative timing of the main diagenetic features can be reconstructed by considering the
286 relationships between the different diagenetic events (Fig. 9). However, there are some
287 diagenetic differences between fluvial and aeolian sandstones.

288 The earliest diagenetic event was the formation of grain coating clays in aeolian deposits,
289 which is considered to be introduced from the infiltration of clay-bearing groundwater
290 through the sands. This event was prior to the compaction and could be proved by the
291 presence of grain coating clays at grain contacts (Figs. 6b and 10).

292 Mechanical compaction in both aeolian and fluvial deposits followed after clay infiltration,
293 during which mica flakes were deformed around quartz and feldspar grains (Fig. 4b). In both
294 fluvial and aeolian samples, an early dolomite cementation occurred at this time, as in some
295 samples the detrital grains appear to float and point grain contact is preserved within the
296 poikilotopic dolomite cement (Fig. 5c). Where dolomite is not present, grains are well
297 compacted (Fig. 5c). The presence of euhedral dolomite with cloudy centres and clear rims
298 (Fig. 5b) might be an indicator of dolomitization occurred on calcrete precursor. Pressure
299 dissolution at quartz grain contacts would have occurred as compaction increased due to the
300 weight of overburden. This is more common in fluvial sandstones possibly due to the greater
301 abundance of rock fragments, such as ductile micaceous clasts, may promote the compaction
302 in the fluvial sandstones and resulted in concavo-convex grain contacts (Fig. 5c). This is also
303 supported by greater maximum COPL value in fluvial samples (29%) than in aeolian samples
304 (22.8%).

305 A subsequent event was the dissolution of feldspar in both aeolian and fluvial deposits
306 which generated authigenic kaolinite (Fig. 4e). Considerable silica ions were released into
307 solution which would form quartz overgrowth in fluvial sandstones, and the pressure
308 dissolution is another possible silica source but only has minor contributions (Tang et al.,
309 2018). This process is usually suggested to be occur in middle to late diagenetic stage
310 (Worden and Morad, 2000). While in the aeolian sandstones, the presence of early-formed
311 grain coating clays provided no site on the grain surface for nucleation of silica ions, quartz
312 overgrowth is thereby almost absent.

313 The whole diagenetic setting might become more alkaline during late diagenesis. In the
314 fluvial sandstone, illitization occurred on kaolinite displaying a fibrous/hairy morphology
315 (Fig. 5f). In the aeolian sandstones, illitization is observed both on grain-coating and pore-
316 filling smectite (Fig. 5i). The presence of pore-bridging habit of illite is often regarded to be
317 an indicator of intermediate to deeper burial (Jiang, 2012). It can also be supported by XRD
318 data (Table 1), the I/S is in R1 ordered interstratification and the percentage of illite within
319 I/S is around 70 – 80%, this usually indicates a temperature condition of 100 – 110°C (e.g
320 Hoffman and Hower, 1979; Huang et al., 1993). There are also minor chloritization due to the
321 presence of Mg^{2+} probably originated from the subsequent dolomite dissolution.

322 **6. Discussion**

323 **6.1 Source of grain coating I/S**

324 The cornflake or honeycomb morphology observed under SEM suggests that the grain
325 coating I/S (also the pore-filling I/S) was transformed from smectitic precursor, as illite
326 originated from kaolinite is more possible to show sheet-like morphology (Pollastro, 1985).
327 Mineralogically, Pittman (1992) deduced that smectite could form an effective dense and
328 continuous grain coat because they nucleate flatly attached to the detrital grain surface and
329 curl away from that surface, the clay developed initially as clay wisps and progressed to clay
330 platelets that formed a root zone, then to an open polygonal box-work and finally to a denser
331 polygonal box-work.

332 In this study, the grain coating I/S has a contrasting distribution pattern that it is only
333 found in aeolian sandstones and absent in fluvial sandstones. Within the given arid/semi-arid
334 aeolian-dominated setting, the fine-grained sandstones with discontinuous wavy laminations
335 commonly indicate a wet interdune or desert lake deposits, which were possibly charged by
336 distal of fluvial distributary system sector (i.e. sand flat) during fluvial-retreat period. As a

337 consequence, the fine-grained sediments, in this case smectitic clays, would be accumulated
338 in this setting and flow into aeolian dune by mechanical infiltration, which is suggested to be
339 a likely main source of grain coating and pore-filling I/S.

340 Petrographic evidence also supports this idea. Wilson (1992) has set several criteria for
341 recognizing mechanically infiltrated clay rims in aeolian and shallow marine sandstones: 1)
342 presence at grain contacts; 2) increased thickness in depressions on framework-grain surface;
343 and 3) more extensive development in finer grained laminae or beds. In this study, the
344 petrographic features of grain coating I/S meet the recognition criteria of mechanical
345 infiltration, it occurs at the grain contacts of aeolian sandstones, and generally shows a
346 thicker I/S coating in the framework-grain depressions and rough surfaces than the non-
347 depression and smooth areas (Fig. 10). Additional evidence from pinstripe laminated dune
348 sandstones clearly displays that more extensive development of grain coating and pore-filling
349 I/S occurred in finer-grained aeolian sands than in medium-grain aeolian sands (Fig. 11).

350 **6.2 Effect of grain coating I/S on reservoir quality**

351 The sum of total cements (dolomite, quartz overgrowth and authigenic clays) clearly has
352 an inverse relationship ($R^2 = 0.47$) with porosity (Fig. 12); this at least indicates that the
353 various types of cementation are jointly the main control of reservoir quality. As the dolomite
354 and authigenic kaolinite occurred in both fluvial and aeolian sandstones, the most remarkable
355 difference between two sandstone types is the quartz overgrowth which is extensively
356 distributed (up to 6%) in fluvial sandstones and nearly negligible in aeolian sandstones.

357 Continuous grain coating minerals are often the key factor for high porosity in deeply
358 buried (> 2.5 km) sandstones (Pittman et al., 1992). Amongst the numerous studies, the grain
359 coating chlorite and microcrystalline quartz are most frequently mentioned (e.g. Pittman and
360 Lumsden, 1968; Ehrenberg, 1993; Aase et al., 1996; Stricker and Jones, 2016). In our study,
361 the grain coating I/S is also effective on inhibiting quartz overgrowth thus preserving porosity.

362 In the Buchan Formation, the amount of quartz cement in all the samples is clearly linked
363 to the presence and coverage of grain coating I/S. The fluvial sandstones do not contain any
364 type of continuous and well developed clay coatings around quartz grains (in the selected
365 sample, grain coverage is nearly 0%, n = 89) and are hence 95% of grains (84 out of 89) are
366 cemented by quartz overgrowth in variable amount (Fig. 13a). Conversely, grain coating I/S
367 are well developed in almost all the aeolian sandstone samples with good coverage (in the
368 selected sample, grain coverage = 100%, n = 212) and continuity, and the quartz cementation
369 is almost absent (Fig. 13b). To quantitatively evaluate the effect of grain coating I/S, we
370 employ the algorithm of Ehrenberg (1993) to calculate the theoretical amount of quartz
371 cementation in upper fine to medium-grained (grain size set as 0.25 mm – 0.3 mm) aeolian
372 sandstones if the grain coating I/S were absent. With the assumed duration of 70 million
373 years from beginning of Palaeogene, the result shows there would be about 6 – 7% porosity
374 has been preserved by grain coating I/S (Fig. 14).

375 The grain coating I/S in this study was transformed from smectitic precursor. For the
376 reservoir quality, smectitic clay usually has two shortcomings: 1) smectite would transform to
377 mixed layer smectite-illite and finally illite when the K^+ is enriched in the fluid and
378 temperature reaches around 70 – 80°C or higher. The hairy/fibrous morphology of illite
379 would reduce the pore and throat space, thus significantly decreasing reservoir quality,
380 especially permeability (e.g. Almon and Davies, 1981; Wilson and Stanton, 1994; Le Gallo et
381 al., 1998); 2) smectite has a high water sensitivity thus could easily swell and occupy the pore
382 space (Gray and Rex, 1965).

383 However, these two shortcomings have very limited impact on reservoir quality in this
384 study. Huang et al. (1993) and Wilson and Stanton (1994) suggested that the kinetics of
385 illitization on precursor detrital smectitic clays not solely depends on temperature but
386 potassium concentration and total time-temperature exposure. In the Buchan Formation,

387 feldspar dissolution might provide considerable amount of K^+ . The burial history has
388 illustrated that the Buchan Formation were consistently at shallow depth (< 1.5 km,
389 temperature $< 70^\circ\text{C}$) until the Palaeogene and was then rapidly buried to present day
390 maximum burial depth. This rapid burial would only provide short thermal exposure which is
391 insufficient for full and complete illitization. Secondly, the amount of pore-filling I/S are
392 commonly less than 5% in aeolian sandstone samples and this would not significantly
393 occlude the pore space.

394 **Conclusions**

395 The grain coatings observed in the fluvial-aeolian Buchan Formation sandstones of the
396 Ardmore Field have been identified as illite/smectite (I/S) which were transformed from
397 smectite precursor. The effect of porosity preservation due to grain coating chlorite and
398 microcrystalline quartz has been demonstrated in a number of publications, this study shows
399 that I/S coatings can also be very effective in preventing quartz cementation under specific
400 conditions, and thereby help preserving primary porosity.

401 In the fluvial sandstones, the precursor material has been absent resulting in the absence of
402 clay coatings on the sand grains, and thereby quartz cementation is extensively developed and
403 reservoir quality is poorer.

404 The thick and continuous grain coating I/S with extensive grain coverage is only observed
405 in aeolian sandstones and this clay coating has inhibited quartz overgrowth and hence high
406 porosity values have been persevered at more than 2.5 km burial depth. The illitization on
407 smectite occurred limitedly thus would not significantly reduce reservoir quality. This is
408 mainly due to the featured burial history: the Buchan Formation was at consistently shallow
409 depth and low temperature until Palaeogene which is not kinetically favourable to activate the
410 smectite illitization. After the Palaeogene, the Buchan Formation was buried to today's

411 maximum depth and temperature rapidly, the short time-temperature exposure is insufficient
412 for full and complete illitization. The I/S coatings were generated from smectitic precursor. It
413 is possible that the precursor has been formed by mechanical infiltration from associated
414 damp interdune deposits possibly charged by clay-bearing water representing distal sector of
415 fluvial distributary system during aeolian-dominated period.

416 The understanding of the positive effect on porosity preservation from grain-coating I/S
417 may aid predictions of high quality Devonian-hosted reservoirs in the North Sea. Such
418 sandstones could form attractive exploration targets that hitherto may have been ignored
419 because they would be expected to have low porosity on the basis of regional trends.

420 **Acknowledgments**

421 The author thanks CGG for providing the seismic data; Enquest PLC for supporting this
422 research through access to core and financial support of analytical work; X-ray Mineral
423 Services Ltd for processing the XRD analysis; Dr Bernard Besly for providing data and
424 helpful discussions; BGS (British Geological Survey) for its assistance in facilitating the
425 examination of Devonian cores. We are all grateful for the expertise and general assistance
426 offered by Mr Ian Chaplin (Department of Earth Sciences, Durham University) and Mr Leon
427 Bowen (Department of Physics, Durham University) in the preparation of samples.

428

429 **REFERENCES**

- 430 Aase, N.E., Bjorkum, P.A. and Nadeau, P.H., 1996. The effect of grain-coating microquartz on
431 preservation of reservoir porosity. *AAPG Bulletin*, 80(10): pp. 1654-1673.
432 Almon, W.R. and Davies, D.K., 1981. Formation damage and the crystal chemistry of clays. Short
433 course in clays and the resource geologist: Montreal, Mineralogical Association of Canada, 7:
434 pp. 81-102.
435 Beard, D. and Weyl, P., 1973. Influence of texture on porosity and permeability of unconsolidated
436 sand. *AAPG Bulletin*, 57(2): pp. 349-369.

- 437 Berger, A., Gier, S. and Krois, P., 2009. Porosity-preserving chlorite cements in shallow-marine
438 volcanoclastic sandstones: Evidence from Cretaceous sandstones of the Sawan gas field,
439 Pakistan. *AAPG Bulletin*, 93(5): pp. 595-615.
- 440 Bifani, R. and Smith, C., 1985. The Argyll field after a decade of production. *Society of Petroleum*
441 *Engineers Journal*, SPE-13987-MS: pp. 1-32.
- 442 Carr, A., 2003. Thermal history model for the South Central Graben, North Sea, derived using both
443 tectonics and maturation. *International Journal of Coal Geology*, 54(1): pp. 3-19.
- 444 Di Primio, R. and Neumann, V., 2008. HPHT reservoir evolution: a case study from Jade and Judy
445 fields, Central Graben, UK North Sea. *International Journal of Earth Sciences*, 97(5): pp.
446 1101-1114.
- 447 Edwards, C., 1991. The Buchan Field, Blocks 20/5a and 21/1a, UK North Sea. In: I.L. Abbotts
448 (Editor), *United Kingdom Oil and Gas Fields, 25 Years Commemorative Volume*. 14.
449 Geological Society, London, pp. 253-259.
- 450 Ehrenberg, S., 1993. Preservation of anomalously high porosity in deeply buried sandstones by grain-
451 coating chlorite: examples from the Norwegian continental shelf. *AAPG Bulletin*, 77(7): pp.
452 1260-1286.
- 453 Folk, R.L., 1957. *Petrology of sedimentary rocks*. Hemphill Publishing Company, pp. 63.
- 454 Gambaro, M. and Currie, M., 2003. The Balmoral, Glamis and Stirling fields, block 16/21, UK
455 Central North Sea. In: J.G. Gluyas and H.M. Hichens (Editors), *United Kingdom Oil and Gas*
456 *Fields Commemorative Millennium Volume*. 20. Geological Society, London, pp. 395-413.
- 457 Glennie, K. and Provan, D., 1990. Lower Permian Rotliegend reservoir of the southern North Sea gas
458 province. In: J. Brooks (Editor), *Geological Society Special Publications: Classic Petroleum*
459 *Provinces*. 50. Geological Society, London, pp. 399-416.
- 460 Gluyas, J.G., Mair, B., Schofield, P., Arkley, P. and McRae, D., 2005. Ardmore Field: rebirth of the
461 first offshore oil field, UKCS, Geological Society, London, *Petroleum Geology Conference*
462 *series*. Geological Society of London, pp. 367-388.
- 463 Gray, D. and Rex, R., 1965. Formation damage in sandstones caused by clay dispersion and migration.
464 In: A. Swineford (Editor), *Clays and Clay Minerals: Proceedings of the Fourteenth National*
465 *Conference*. pp. 355-365.
- 466 Hoffman, J. and Hower, J., 1979. Clay mineral assemblages as low grade metamorphic
467 geothermometers: application to the thrust faulted disturbed belt of Montana, USA. In: P.A.
468 Scholle, & Schluger, P. R. (Editor), *Special Publications of SEPM: Aspects of diagenesis:*
469 *based on symposia*. 26, pp. 55-79.
- 470 Howell, J. and Mountney, N., 1997. Climatic cyclicality and accommodation space in arid to semi-arid
471 depositional systems: an example from the Rotliegend Group of the UK southern North Sea.
472 In: K. Ziegler, P. Turner and S.R. Daines (Editors), *Geological Society Special Publications:*
473 *Petroleum Geology of the Southern North Sea: Future Potential*. 123. Geological Society,
474 London, pp. 63-86.
- 475 Huang, W.-L., Longo, J.M. and Pevear, D.R., 1993. An experimentally derived kinetic model for
476 smectite-to-illite conversion and its use as a geothermometer. *Clays and Clay Minerals*, 41: pp.
477 162-162.
- 478 Jiang, S., 2012. Clay minerals from the perspective of oil and gas exploration. In: M. Valaškova and
479 G.S. Martynkova (Editors), *Clay Minerals in Nature-Their Characterization, Modification and*
480 *Application*. InTech, pp. 21-38.
- 481 Kearsey, T., Ellen, R., Millward, D. and Monaghan, A., 2015. Devonian and Carboniferous
482 stratigraphical correlation and interpretation in the Central North Sea, Quadrants 25–44.
483 *British Geological Survey (CR/15/117N) (Unpublished)*: pp. 1-80.
- 484 Knight, I., Allen, L., Coipel, J., Jacobs, L. and Scanlan, M., 1993. The Embla Field, Geological
485 Society, London, *Petroleum Geology Conference series*. Geological Society of London, pp.
486 1433-1444.
- 487 Le Gallo, Y., Bildstein, O. and Brosse, E., 1998. Coupled reaction-flow modeling of diagenetic
488 changes in reservoir permeability, porosity and mineral compositions. *Journal of Hydrology*,
489 209(1): pp. 366-388.
- 490 Leveille, G.P., Primmer, T.J., Dudley, G., Ellis, D. and Allinson, G.J., 1997. Diagenetic controls on
491 reservoir quality in Permian Rotliegendes sandstones, Jupiter Fields area, southern North Sea.

492 In: K. Ziegler, P. Turner and S.R. Daines (Editors), Geological Society Special Publications:
493 Petroleum Geology of the Southern North Sea: Future Potential. 123. Geological Society,
494 London, pp. 105-122.

495 Lundergard, P., 1992. Sandstone porosity loss. A “big picture” view of the importance of
496 Compaction. *Journal of Sedimentary Petrology*, 62: pp. 250-260.

497 Nagtegal, P., 1979. Relationship of facies and reservoir quality in Rotliegendes desert sandstones,
498 southern North Sea region. *Journal of Petroleum Geology*, 2(2): pp. 145-158.

499 Nguyen, B.T., Jones, S.J., Goult, N.R., Middleton, A.J., Grant, N., Ferguson, A. and Bowen, L.,
500 2013. The role of fluid pressure and diagenetic cements for porosity preservation in Triassic
501 fluvial reservoirs of the Central Graben, North Sea. *AAPG Bulletin*, 97(8): pp. 1273-1302.

502 Pittman, E.D., 1972. Diagenesis of quartz in sandstones as revealed by scanning electron microscopy.
503 *Journal of Sedimentary Petrology*, 42(3): pp. 507-519.

504 Pittman, E.D., Larese, R.E. and Heald, M.T., 1992. Clay coats: Occurrence and relevance to
505 preservation of porosity in sandstones. In: D.W. Houseknecht and E.D. Pittman (Editors),
506 Special Publications of SEPM: Origin, Diagenesis, and Petrophysics of Clay Minerals in
507 Sandstones. 47, pp. 241-255.

508 Pittman, E.D. and Lumsden, D.N., 1968. Relationship Between Chlorite Coatings on Quartz Grains
509 and Porosity, Spiro Sand, Oklahoma: NOTES. *Journal of Sedimentary Petrology*, 38(2): pp.
510 668-670.

511 Purvis, K., 1992. Lower Permian Rotliegend sandstones, southern North Sea: a case study of
512 sandstone diagenesis in evaporite-associated sequences. *Sedimentary Geology*, 77(3-4): pp.
513 155-171.

514 Robinson, A., Coleman, M.L. and Gluyas, J.G., 1993. The age of illite cement growth, Village Fields
515 area, southern North Sea: Evidence from K-Ar ages and 18O/16O ratios. *AAPG Bulletin*,
516 77(1): pp. 68-80.

517 Robson, D., 1991. The Argyll, Duncan and Innes Fields, Block 30/24 and 30/25a, UK North Sea. In:
518 I.L. Abbotts (Editor), United Kingdom Oil and Gas Fields, 25 Years Commemorative
519 Volume. 14. Geological Society, London, pp. 219-226.

520 Stanton, P.T. and Wilson, M.D., 1994. Measurement of Independent Variables-Composition. In: M.D.
521 Wilson (Editor), Special Publications of SEPM: Reservoir Quality Assessment and Prediction
522 in Clastic Rocks (SC30). Short Course Notes, pp. 277-290.

523 Storvoll, V., Bjørlykke, K., Karlsen, D. and Saigal, G., 2002. Porosity preservation in reservoir
524 sandstones due to grain-coating illite: a study of the Jurassic Garn Formation from the Kristin
525 and Lavrans fields, offshore Mid-Norway. *Marine and Petroleum Geology*, 19(6): pp. 767-
526 781.

527 Stricker, S. and Jones, S.J., 2016. Enhanced porosity preservation by pore fluid overpressure and
528 chlorite grain coatings in the Triassic Skagerrak, Central Graben, North Sea, UK. In: P.J.
529 Armitage, A.R. Butcher, J.M. Churchill, A.E. Csoma, C. Hollis, R.H. Lander, J.E. Omma and
530 R.H. Worden (Editors), Geological Society Special Publications: Reservoir Quality of Clastic
531 and Carbonate Rocks: Analysis, Modelling and Prediction. 435, pp. 1-21.

532 Swarbrick, R., Osborne, M., Grunberger, D., Yardley, G., Macleod, G., Aplin, A., Larter, S., Knight, I.
533 and Auld, H., 2000. Integrated study of the Judy Field (Block 30/7a)—an overpressured
534 Central North Sea oil/gas field. *Marine and Petroleum Geology*, 17(9): pp. 993-1010.

535 Sweet, M., 1999. Interaction between aeolian, fluvial and playa environments in the Permian Upper
536 Rotliegend Group, UK southern North Sea. *Sedimentology*, 46(1): pp. 171-188.

537 Tang, L., Gluyas, J.G. and Jones, S.J., 2018. Diagenetic and geochemical studies of the Buchan
538 Sandstone (Upper Devonian) in the Central North Sea. *Petroleum Science*, in press.

539 Wilson, M.D., 1992. Inherited grain-rimming clays in sandstones from eolian and shelf environments:
540 their origin and control on reservoir properties. In: D.W. Houseknecht and E.D. Pittman
541 (Editors), Special Publications of SEPM: Origin, Diagenesis, and Petrophysics of Clay
542 Minerals in Sandstones. 47, pp. 209-225.

543 Wilson, M.D. and Stanton, P.T., 1994. Diagenetic mechanisms of porosity and permeability reduction
544 and enhancement. In: M.D. Wilson (Editor), Special Publications of SEPM: Reservoir Quality
545 Assessment and Prediction in Clastic Rocks (SC30). Short Course Notes, pp. 59-118.

546 Wilson, M.J., Wilson, L. and Patey, I., 2014. The influence of individual clay minerals on formation
547 damage of reservoir sandstones: a critical review with some new insights. *Clay Minerals*,
548 49(2): pp. 147-164.
549 Worden, R.H. and Morad, S., 2000. Quartz Cementation in Oil Field Sandstones: A Review of the
550 Key Controversies. In: R.H. Worden and S. Morad (Editors), *International Association of*
551 *Sedimentologists Special publication: Quartz cementation in sandstones*. 29, pp. 1-20.

552

553

554

555

556

557

558

559 **APPENDIX**

560

561 **Supplementary table 1.** Petrography information of the Buchan Formation samples in
562 Ardmore field, note the well names and locations are shown in Fig. 1a in bold.

563

564 **Supplementary table 2.** Total cement volume (C), measured porosity (Pm), intergranular
565 volume (IGV), porosity-loss by mechanical compaction (COPL) and porosity-loss by
566 cementation (CEPL) all in% for the aeolian dune and braided channel samples

567

568

569 **LIST OF TABLES AND FIGURES**

570

571 **Table. 1.** XRD data for < 2 µm size mineral fraction in selected samples.

572

573 **Fig. 1.** Geological maps showing: (a) Location and main structure elements of Ardmore
574 (Adm) Field; (b) Vertical section of an SW-NE profile (dashed line in 1a); (c) Seismic
575 section of an SW-NE profile (part of dashed line in 1a).

576 **Fig. 2.** General stratigraphy of the Ardmore Field and a schematic stratigraphic log of the
577 Buchan Formation.

578 **Fig.3.** (a) QFR charts for fluvial sandstone samples; (b) QFR charts for aeolian sandstone
579 samples.

580 **Fig. 4.** Photomicrographs of sandstone detrital minerals. All thin section images were
581 produced under cross-polarized light. (a) Monocrystalline quartz grain with quartz
582 overgrowth and visible dust rims (yellow arrows) on the original detrital grain. Well 30/24-34,
583 2967.8 m, unit B11, fluvial facies; (b) Bent muscovite grains (white arrows) and quartz grains
584 with undulose extinction. Well 30/24-20z, 3125.4 m, unit B04, fluvial facies; (c)
585 Polycrystalline quartz in a fine pebble grain. Well 30/24-28, 2795 m, unit B10, fluvial facies;
586 (d) Microcline with polysynthetic twinning, note the presence of carbonate cement and pore-
587 filling kaolinite. Well 30/24-05, 2846.4 m, unit B04, fluvial facies; (e) SEM image of
588 severely dissolved feldspar and authigenic kaolinite. Well 30/24-20z, 3125.4 m, unit B04,
589 fluvial facies; (f) Possible volcanic-origin rock fragments, note the pore-filled kaolinite
590 aggregates and quartz overgrowth (yellow arrows). Well 30/24-05, 2847 m, unit B04, fluvial
591 facies;

592 Q-quartz; Qu- quartz grains with undulose extinction; PQ- Polycrystalline quartz; F-
593 feldspar; C-carbonate cement; K-kaolinite; RF-rock fragment

594 **Fig. 5.** Photomicrographs showing different diagenetic minerals. (a) Thin bands of ‘spotty’
595 red-brown stained cements (yellow arrows) in the cores. Well 30/24-05, 2849.1 m, unit B04,
596 fluvial facies; (b) Dolomite cements in the pore space showing well rhombic shape with
597 cloudy core and light rims, cross-polarized light, well 30/24-05, 2849.1 m, unit B04, fluvial
598 facies; (c) Quartz grains floating in the dolomite cements and well compacted (white arrows)
599 without pore-filling dolomite cements, cross-polarized light, well 30/24-20z, 3126 m, unit
600 B04, fluvial facies; (d) Extensive quartz overgrowth (red arrows) on the detrital quartz grains,
601 cross-polarized light, well 30/24-20z, 3126 m, unit B04, fluvial facies; (e) Kaolinites showing
602 pseudo-hexagonal plates and vermicular and booklet morphologies under SEM. Well 30/24-
603 20z, 3176.6 m, unit B04, fluvial facies; (f) Fibrous/hairy authigenic illite based on kaolinite
604 under SEM. Well 30/24-20z, 3126 m, unit B04, fluvial facies; (g) SEM image showing pore-
605 bridging habit of authigenic illite (yellow arrows). Well 30/24-20z, 3165.3 m, fluvial facies;
606 (h) Grain coating clays existing at grain contacts (white arrows), plane- polarized light ,well
607 30/24-31, 3197.7 m, unit B08, aeolian facies; (i) Pore-filling and grain coating smectite-illite
608 mixed layers showing honeycomb or cornflake morphology under SEM. Well 30/24-28,
609 2891.6 m, unit B07, aeolian facies; (j) Enlarged view of the rectangle area in Fig. 6i, note the
610 filamentous terminations (white arrows) indicates the illitization occurred; (k) EDX spectrum
611 of the rectangle area in Fig. 6j, note the small peak of potassium indicates the partial
612 illitization.

613 D-dolomite; P-pore space; K-kaolinite; I-illite; I/S-illite/smectite

614 **Fig. 6.** The mineral phase map of a typical aeolian dune sandstone sample which contain
615 well-developed and continuous grain coating clays. (a) BSEM image of the thin section; (b)

616 Grain coating phase map. Sample from Well 30/24-28, 2891.6 m, unit B07, aeolian dune
617 facies.

618 **Fig. 7.** Porosity and permeability distributions and correlation coefficients for: (a) All the
619 samples; (b) Stratigraphic unit B04; (c) Stratigraphic unit B09; (d) Stratigraphic unit B10; (e)
620 Stratigraphic unit B11; (f) Stratigraphic units B07 and B08.

621 **Fig. 8.** 1D burial depth curve with geothermal isochore lines of Buchan Formation in the
622 Ardmore Field.

623 **Fig.9.** Paragenetic sequences of the Buchan Formation, the solid/dash lines represent the
624 major/minor events. Note the superscripts at the end of each event represent: A – the event
625 mainly occurred in aeolian sandstones; F – the event mainly occurred in fluvial sandstones;
626 A&F – the event mainly occurred in both aeolian and fluvial sandstones; * – the event is not
627 observed under either thin section or SEM, but confirmed by XRD.

628 **Fig. 10.** The photomicrograph (plane-polarized light) illustrates the presence of grain
629 coating I/S in the grain contact areas (white arrows), thicker coats in grain surface
630 depressions (yellow arrows) and grain rough surface (red arrows), and thinner coats in non-
631 depression areas (black arrows). Sample from well 30/24-31, 3190.6 m, unit B08, aeolian
632 dune sands.

633

634 **Fig. 11.** Photomicrograph illustrating different abundance of infiltrated clays in a
635 representative pin-stripe lamination dune sandstone sample. Note the finer grain-size
636 lamination (right) clearly contains more pore-filling clays. Well 30/24-31, 3190.6 m, unit
637 B08, aeolian dune sands.

638

639 **Fig. 12.** The scattered porosity and total cements showing a clearly inverse relationship.

640 The data is categorized by aeolian and fluvial facies.

641

642 **Fig. 13.** Comparison between: (a) Fluvial channel sandstone without clay coatings which

643 is extensively cemented by quartz overgrowth, the clay coating coverage is 0%, and about 95%

644 of grains have quartz overgrowth, $n = 89$. Well 30/24-20z, 3117.8 m, unit B04; (b) Aeolian

645 sandstone with very high clay coating coverage (100%, $n = 212$) with no quartz overgrowth.

646 Well 30/24-31, 3202.2 m, unit B08. Both figures were taken under plane-polarized light.

647

648 **Fig. 14.** Empirical calculation of possible quartz overgrowth amounts for sand grain size

649 in 0.25 and 0.30 mm during 70 million years. The algorithm is after Ehrenberg (1993).

650

651 **Table**

652 **Table 1.** XRD data for <2µm size mineral fraction in selected samples

Well	Depth (m)	Facies	Wt.% <2µm	Illite/smectite				Illite			Kaolinite			Chlorite			Quartz		Calcite		Dolomite	
				% A	% B	Order	% I	% A	% B	Crys	% A	% B	Crys	% A	% B	Crys	% A	% B	% A	% B	% A	% B
30/24-28	2790.1	AD	1.9	34.4	0.7	O	70-80	58.3	1.1	P	0.0	0.0	-	7.1	0.1	P	0.3	0.1	0.0	0.0	0.0	0.0
30/24-28	2829.8	AD	3.0	46.3	1.4	O	70-80	25.9	0.8	P	22.6	0.7	M	2.9	0.1	M	2.4	0.1	0.0	0.0	0.0	0.0
30/24-28	2844.1	AD	3.0	50.5	1.5	O	70-80	32.7	1.0	P	7.5	0.2	M	3.5	0.1	M	5.8	0.2	0.0	0.0	0.0	0.0
30/24-31	3190.3	AD	2.0	44.8	0.9	O	70-80	34.9	0.7	P	10.7	0.2	M	5.1	0.1	P	4.5	0.1	0.0	0.0	0.0	0.0
30/24-28	2794.7	CHB	3.3	TR	TR	-	-	22.0	0.7	P	58.7	1.9	M	15.8	0.5	M	3.6	0.1	0.0	0.0	0.0	0.0
30/24-05	2849.3	CHB	3.2	TR	TR	-	-	8.5	0.3	P	72.6	2.3	M	5.3	0.2	P	3.1	0.1	0.0	0.0	10.6	0.3

Facies: AD = aeolian dune; CHB- channel bar

A = Weight% relevant size fraction; B = Weight% bulk sample;

Mixed-layer Ordering: RI= Randomly Interstratified (R0); O = Ordered Interstratification (R1); LR = Long-range Ordering (R3);

Crystallinity: VW = Very Well Crystallised; W = Well Crystallised; M = Moderately Crystallised; P = Poorly Crystallised.

653

654 **Fig 1**

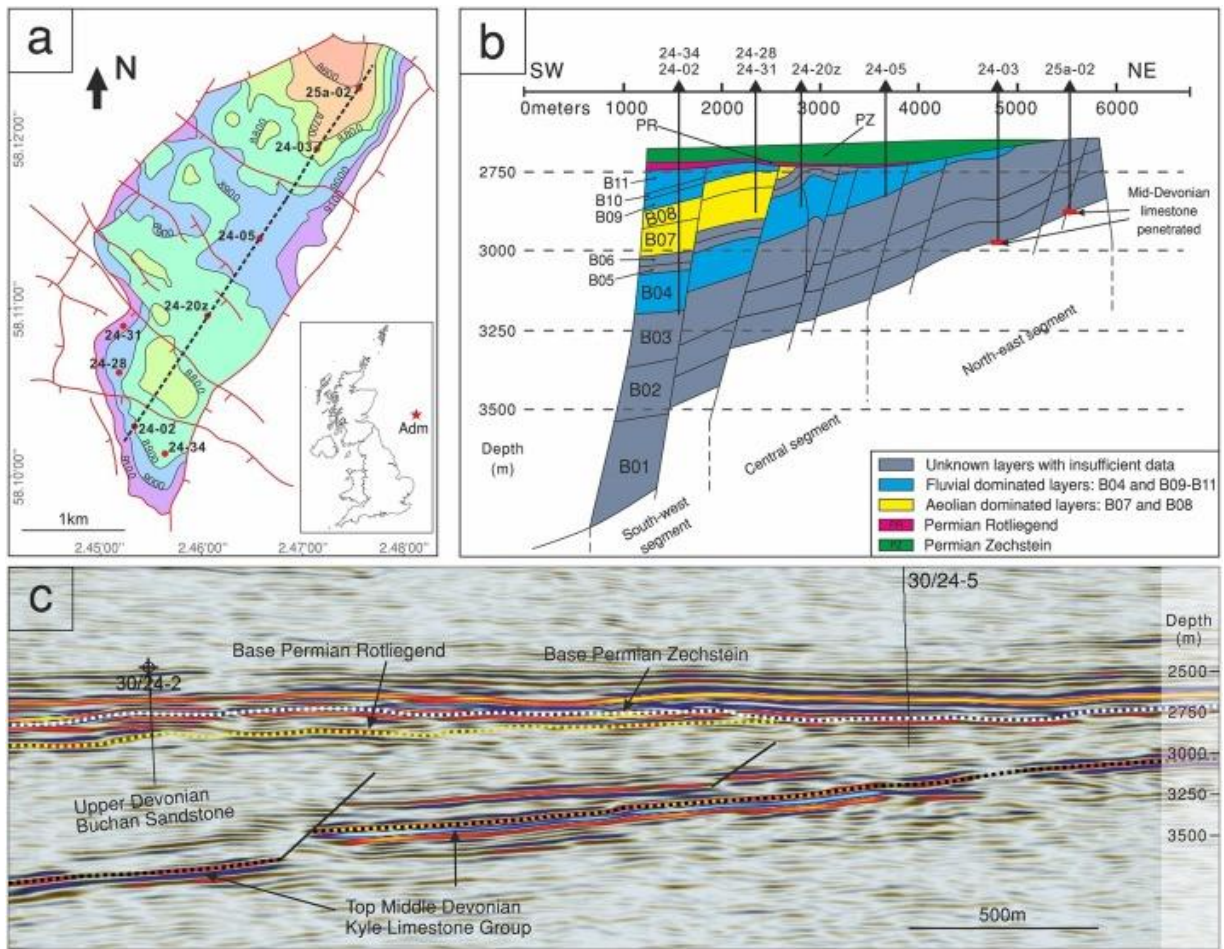
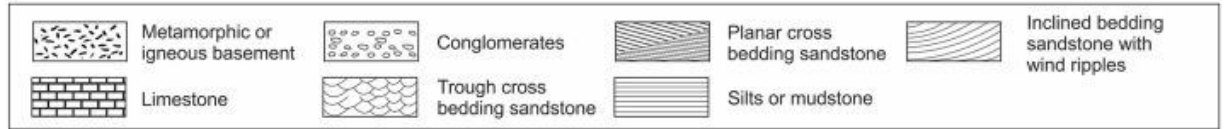
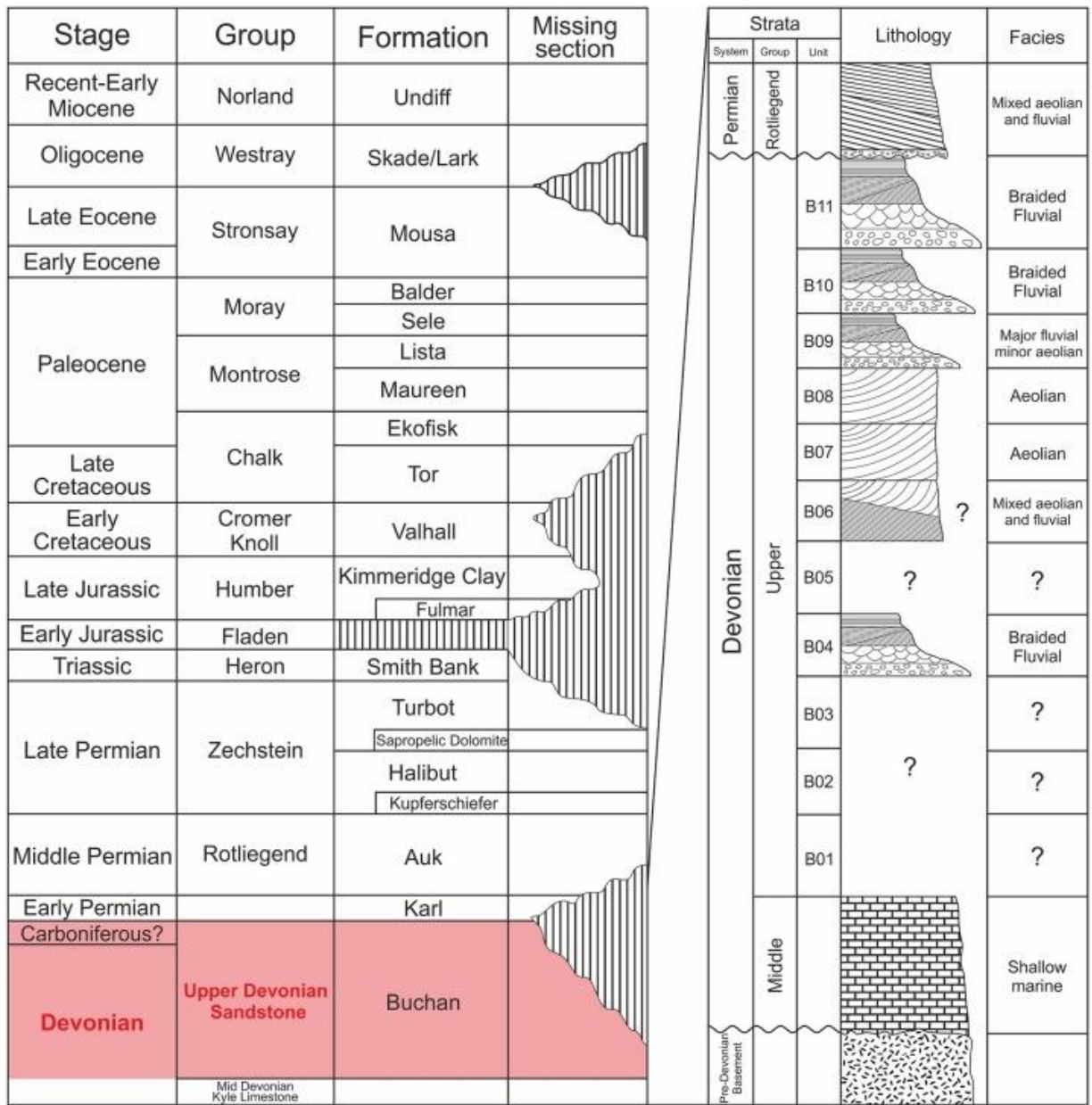
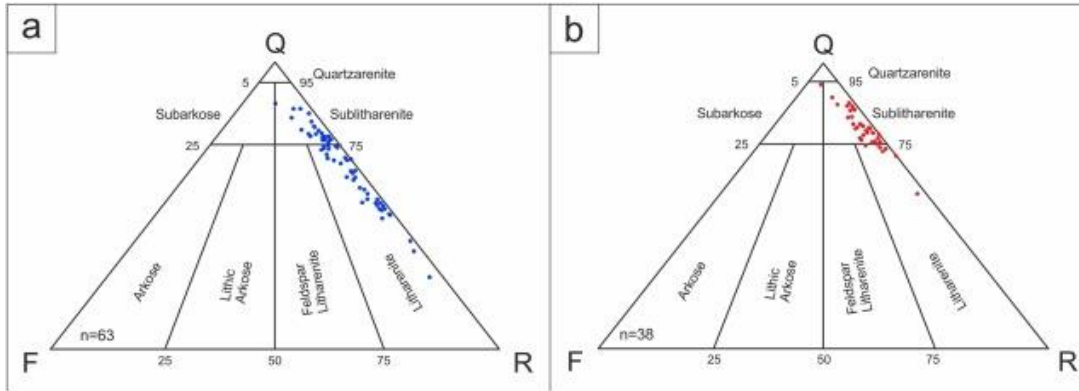


Fig 2

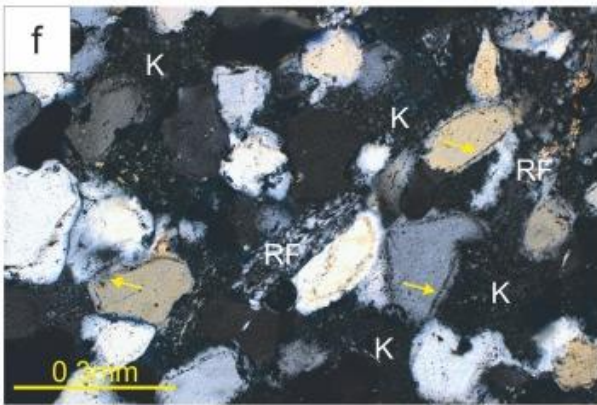
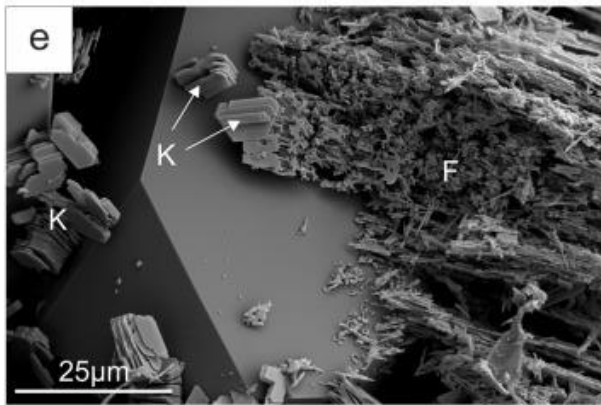
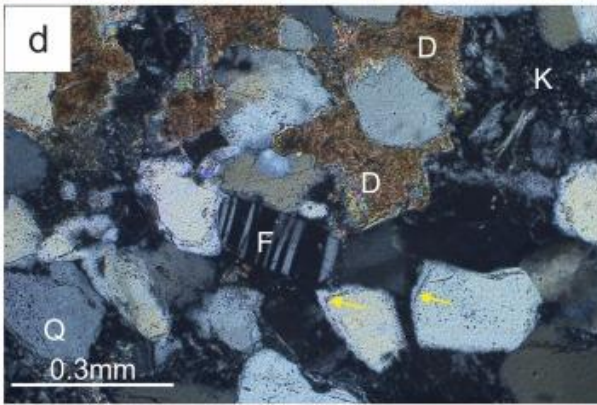
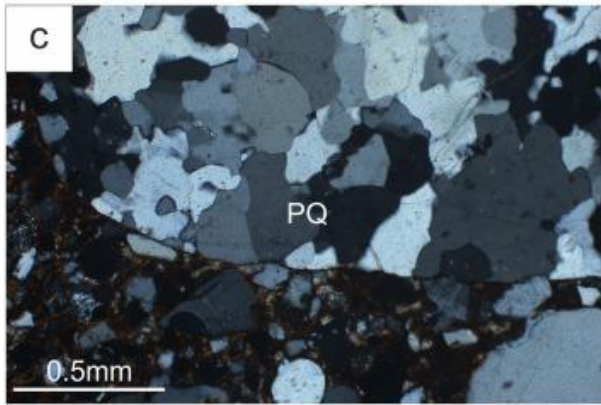
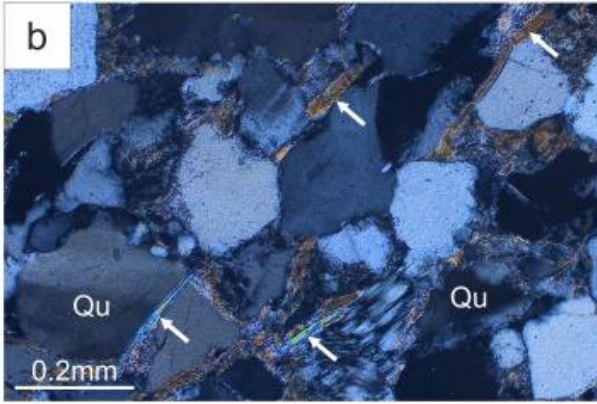
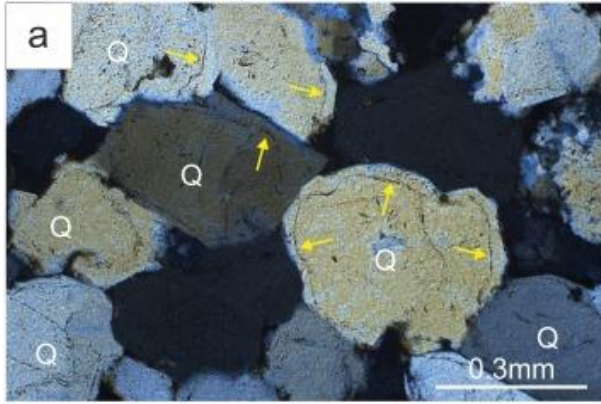


658 Fig 3

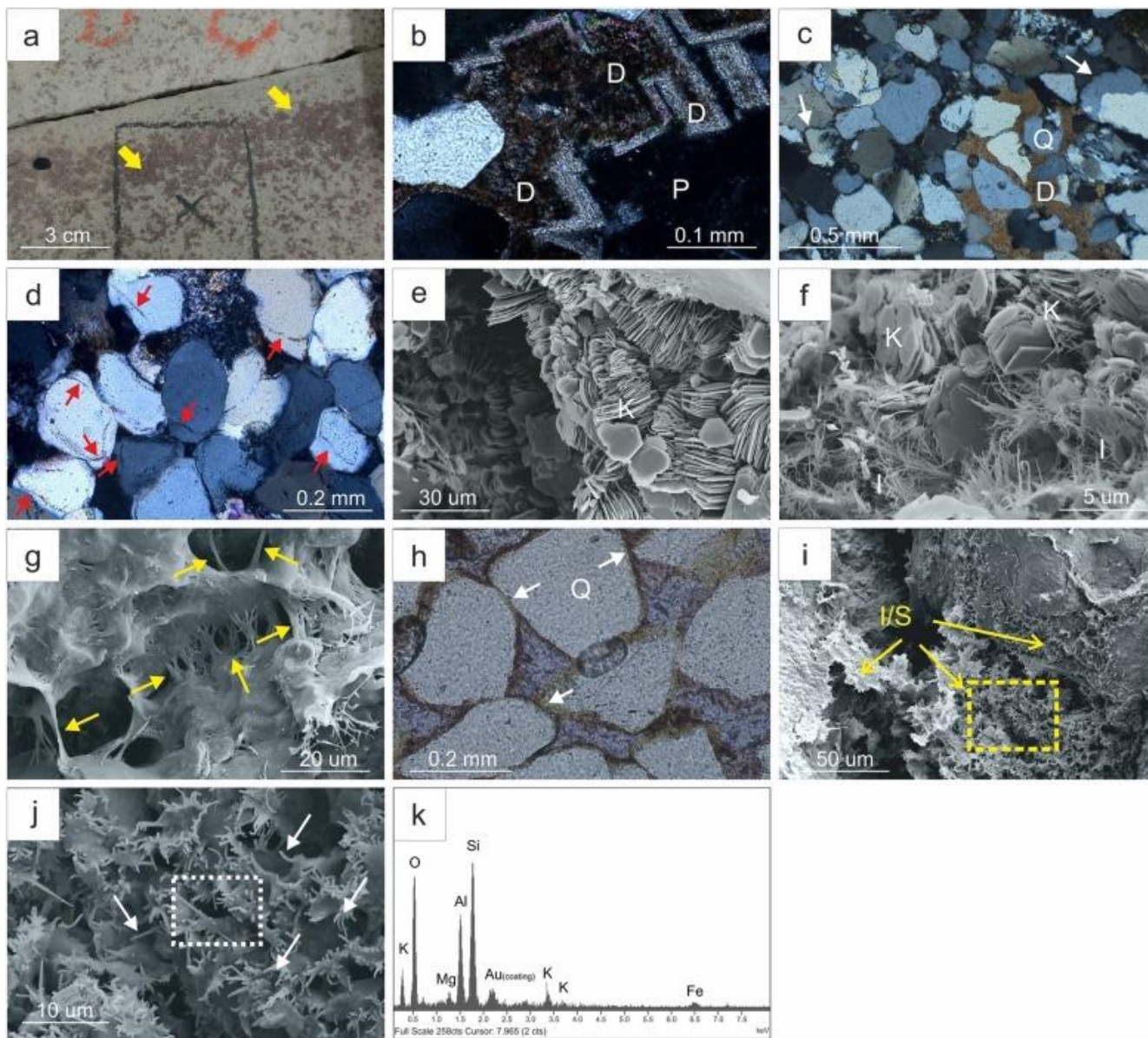


659

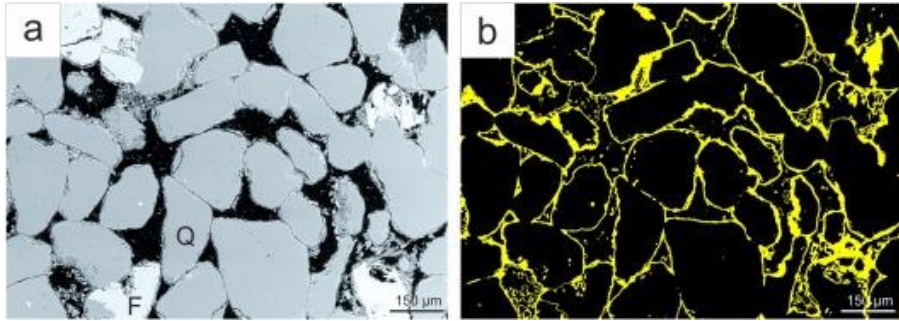
660 Fig 4



662 Fig 5

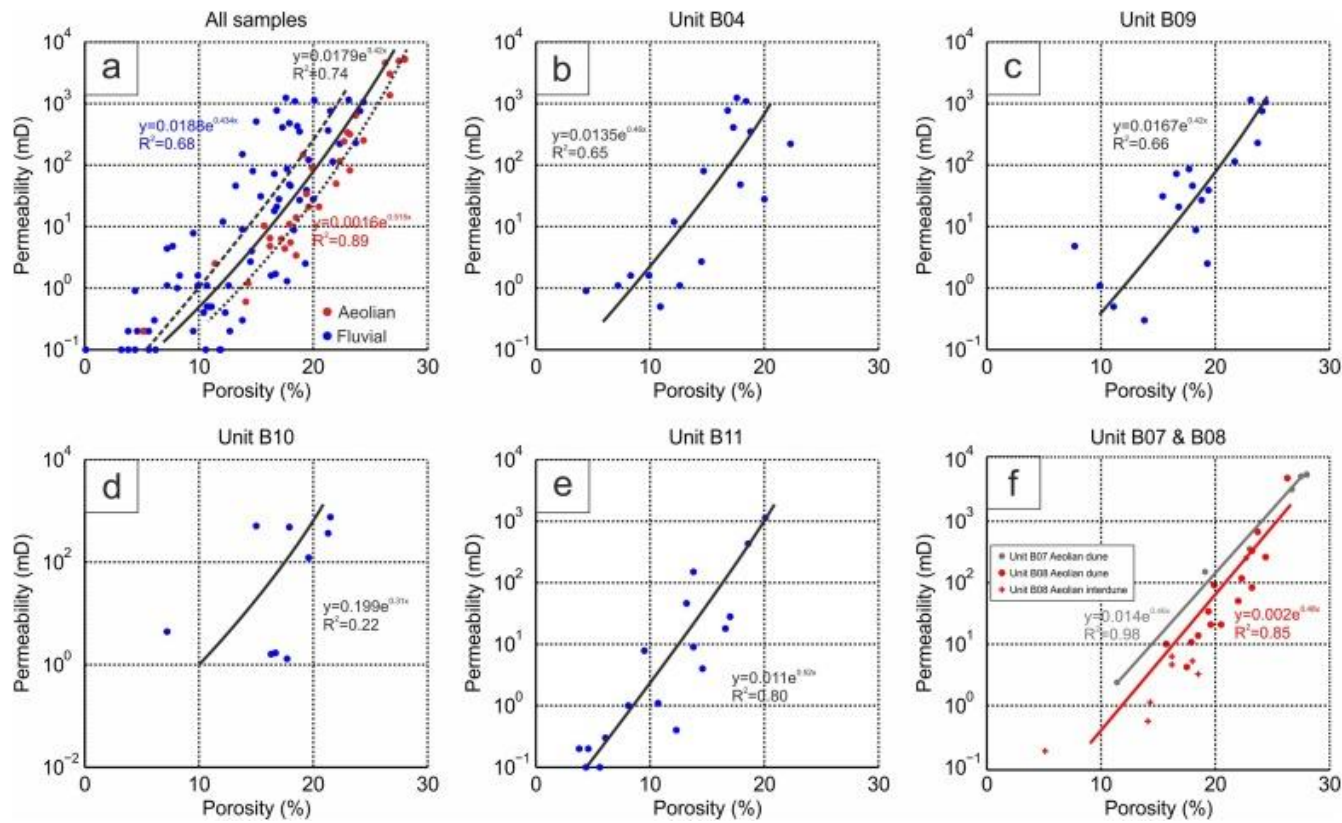


664 Fig 6



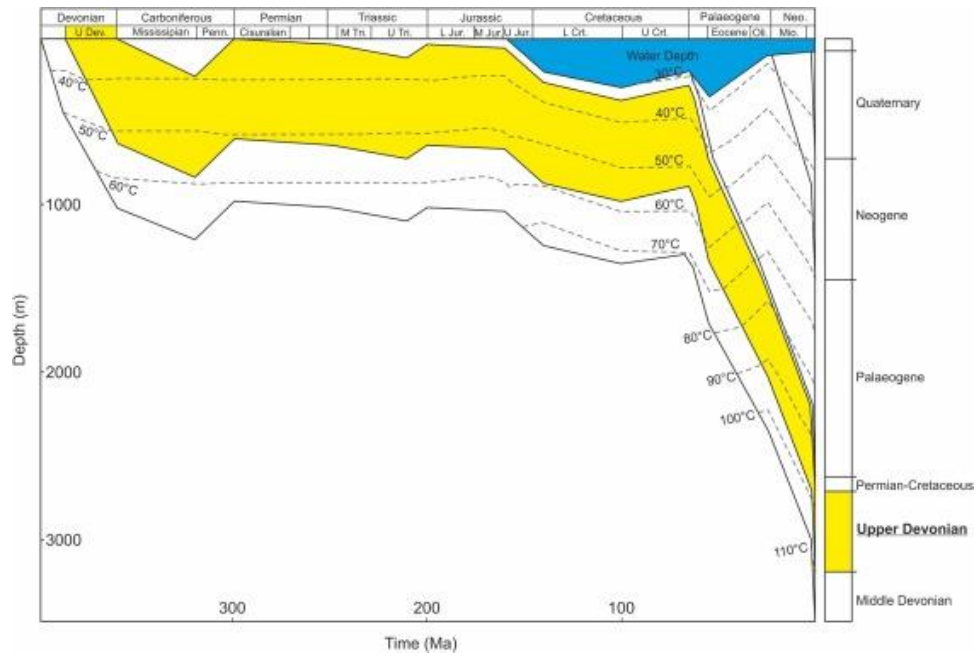
665

666 Fig 7



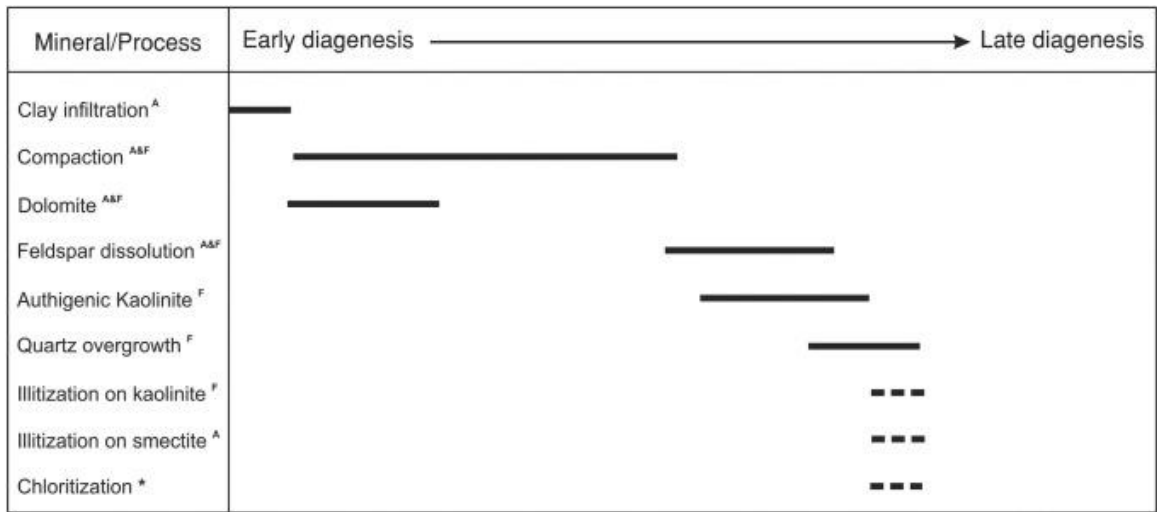
667

668 Fig 8



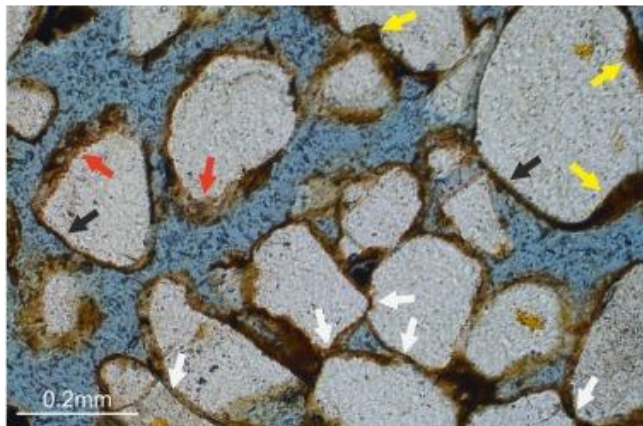
669

670 Fig 9



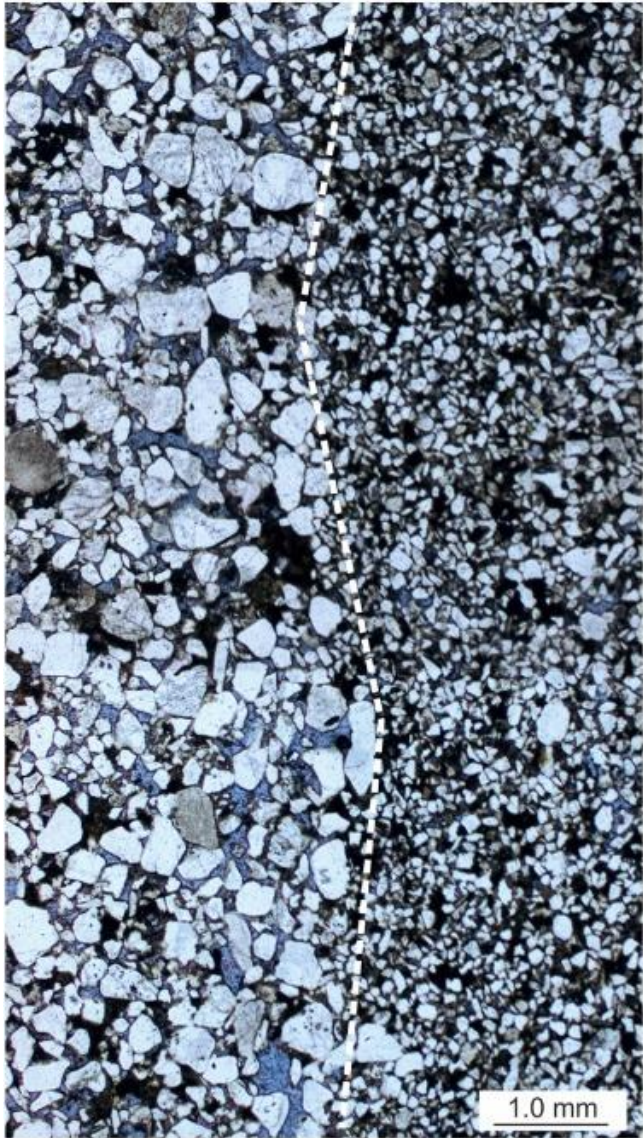
671

672 Fig 10



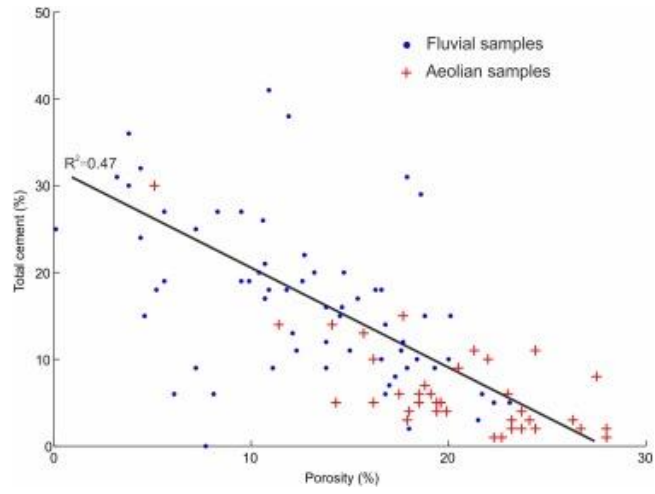
673

674 Fig 11



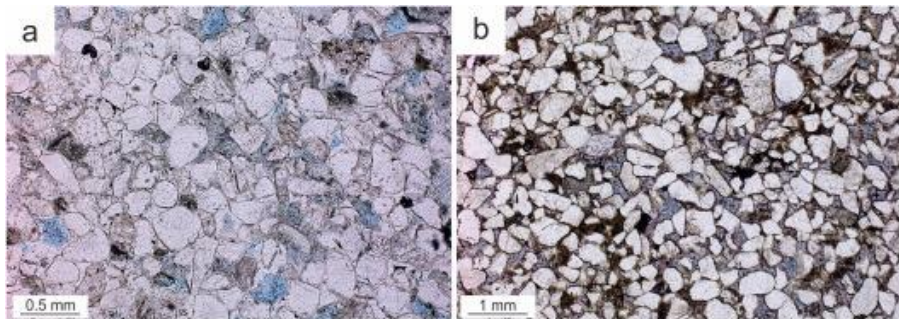
675

676 Fig 12



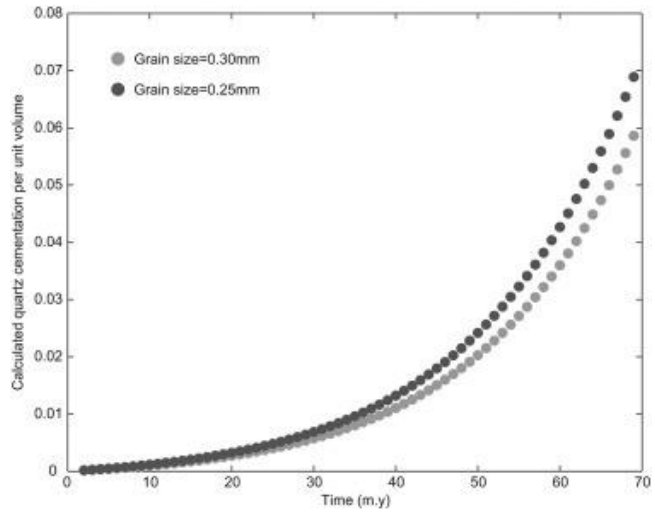
677

678 Fig 13



679

680 Fig 14



681